Cell adhesion and cortex contractility determine cell patterning in the *Drosophila* retina

Jos Käfer*†, Takashi Hayashi‡§¶, Athanasius F. M. Marée‖, Richard W. Carthew§, and François Graner*

*Laboratoire de Spectrométrie Physique, Unité Mixte de Recherche 5588, Université Joseph-Fourier Grenoble I and Centre National de la Recherche Scientifique, 140 Avenue de la Physique, 38402 Saint Martin d'Hères, France; §Department of Biochemistry, Molecular Biology, and Cell Biology, Northwestern University, Evanston, IL 60208; ¶Department of Biophysics and Biochemistry, Graduate School of Science, University of Tokyo, Tokyo 113-0033, Japan; and ‖Theoretical Biology/Bioinformatics, Utrecht University, Padualaan 8, 3584 CH Utrecht, The Netherlands

Edited by Ruth Lehmann, New York University Medical Center, New York, NY, and approved October 1, 2007 (received for review May 7, 2007)

Because of the resemblance of many epithelial tissues to densely packed soap bubbles, it has been suggested that surface minimization, which drives soap bubble packing, could be governing cell packing as well. We test this by modeling the shape of the cells in a *Drosophila* retina ommatidium. We use the observed configurations and shapes in wild-type flies, as well as in flies with different numbers of cells per ommatidia, and mutants with cells where E- or N-cadherin is either deleted or misexpressed. We find that surface minimization is insufficient to model the experimentally observed shapes and packing of the cells based on their cadherin expression. We then consider a model in which adhesion leads to a surface increase, balanced by cell cortex contraction. Using the experimentally observed distributions of E- and N-cadherin, we simulate the packing and cell shapes in the wild-type eye. Furthermore, by changing only the corresponding parameters, this model can describe the mutants with different numbers of cells or changes in cadherin expression.

cell shape | surface mechanics | Cellular Potts model

Cell adhesion molecules are necessary to form a coherent multicellular organism. Not only do they hold cells together, but also differential expression of different types of these molecules plays a central role during development. Members of the cadherin family are the most widespread molecules that mediate adhesion among animal cells, and their role has been demonstrated in, e.g., cell sorting, migration, tumor invasibility, cell intercalation, packing of epithelial cells, axon outgrowth, and more (1–6). We focus here on the role of adhesion in the determination of epithelial cell shape (7).

In the compound eye of *Drosophila*, the basic unit, the ommatidium, is repeated ≈800 times. All ommatidia have the same cell packing, which is essential for correct vision. The ommatidium consists of four cone cells (C cells), which are surrounded by two larger primary pigment cells (P cells). These "units" are embedded in a hexagonal matrix, which consists of secondary and tertiary pigment cells and bristles [see supporting information (SI) Fig. 7; ref. 8].

Two of us (9) showed that cadherin expression influences ommatidial C cell packing. Two cadherin types, E- and N-cadherin, are expressed in different cells: all interfaces bear E-cadherin, whereas N-cadherin is present only at interfaces between the four C cells (SI Fig. 7). Cadherin-containing adherens junctions form a zone close to the apical cell surface, allowing the retina epithelium to be treated as a 2D tissue. In the wild-type and in *Roi*-mutant ommatidia with two to six C cells, these cells assume a packing (or topology, that is, relative positions of cells) strikingly similar to that of a soap-bubble cluster. When cadherin expression is changed in a few or all of the cells, the topology can change. More frequently, only the geometry (individual cell shapes, contact angles at the vertices, interface lengths) changes.

The soap films between bubbles are always under a positive tension, $\gamma>0$. This surface tension describes the energy cost of a unit of interface between bubbles and drives their packing. At equilibrium, in a 2D foam layer, soap bubbles meet by three at each vertex, because four-bubble vertices are unstable (10, 11). In addition, because γ is constant and the same for all interfaces, bubble walls meet at equal (i.e., 120°) angles. More precisely, the surface energy (or rather the perimeter energy for a 2D foam) is γP, where P is the total perimeter of soap films. The foam reaches equilibrium when it minimizes P (because γ is constant), balanced by another constraint fixing each bubble's area.

It has been proposed that cells minimize their surface, like soap bubbles (12–14). Because the surface mechanics of bubbles are quite simple, they can easily be described in a model. However, calculating the equilibrium shape of a cluster of more than four bubbles is difficult (13); for this purpose, we use a numerical method (15, 16) to test whether cell patterning is based on surface minimization. In this first model, the only biological ingredient is differential adhesion (1, 13, 17); an interface between two cells has a constant tension that is lower when the adhesion is stronger (15, 16).

Cells, however, differ greatly from bubbles, in both their membrane and internal composition. Surface tension has been shown to be determined to a large extent by the cortical cytoskeleton (18–21). Adhesive cells have a tendency to increase their contact interfaces (22), not to minimize them. Lecuit and Lenne (14) recently reviewed a large number of experiments and showed that a cell's surface tension results from the opposite actions of adhesion and cytoskeletal contraction. These are the ingredients of a second model (23, 24).

Our approach is to find out whether the observed cell packings and shapes can be described with one of these models, based on the knowledge we have from the experiments. With minimal and realistic assumptions, only the second model reproduces the topology and geometry of the wild-type and mutant ommatidia.

This shows that the competition between adhesion and cell cortex tension is needed to describe this specific cell pattern. We thus confirm and refine the conclusion that surface mechanics are involved in the establishment of cell topology and geometry. Adhesion plays an important role therein, but its role can be understood only when taking into account the effect of the cortical cytoskeleton.

Results

Model Simulations. Why certain shapes are observed more often than others depends on the developmental history of the tissue,

Author contributions: R.W.C. and F.G. designed research; J.K. and T.H. performed research; J.K. and A.F.M.M. contributed new reagents/analytic tools; J.K., T.H., R.W.C., and F.G. analyzed data; and J.K., A.F.M.M., and F.G. wrote the paper.

The authors declare no conflict of interest.

This article is a PNAS Direct Submission.

Abbreviations: C cell, cone cell; P cell, primary pigment cell; MCS, Monte Carlo time step.

†To whom correspondence should be addressed. E-mail: jkafer@spectro.ujf-grenoble.fr.

‡Present address: Department of Zoology, Michigan State University, 203 Natural Science, East Lansing, MI 48824.

This article contains supporting information online at www.pnas.org/cgi/content/full/0704235104/DC1.

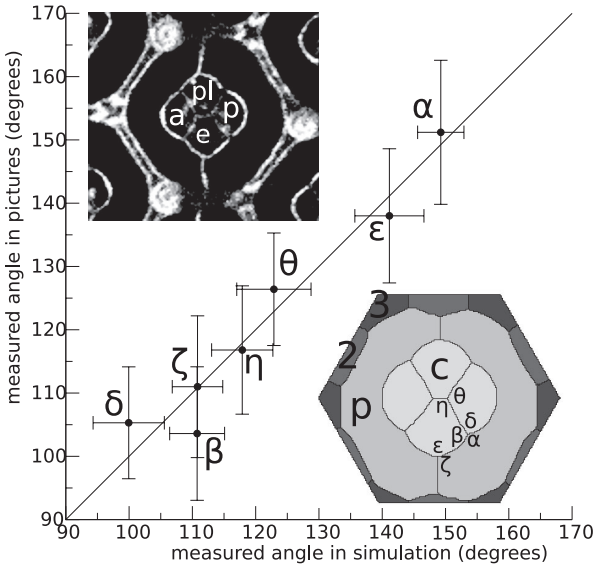

Fig. 1. Wild type. Contact angles measured in experiments and in simulations are plotted as average ± statistical SD; the straight line represents $y = x$. (*Inset Left*) An ommatidium stained for E-cadherin; anterior (a), posterior (p), polar (pl), and equatorial (e) C cells. (*Inset Right*) Variable tension model simulation, with C cells (C) and primary (P), secondary (2), and tertiary (3) pigment cells. One ommatidium contains four times the angles α, β, δ, η, and ζ and two times ε and θ.

which is determined, e.g., by the sequence of cell differentiation and cell divisions and deaths. Because much is still unknown about the developmental history, we do not include it in the modeling. However, because cells seem in mechanical equilibrium at any moment in development (cf. ref. 14), future insights in developmental gene regulation could be translated in parameter changes that permit the modeling of the dynamics of development.

Simulations thus start from unstable initial conditions (SI Fig. 8) designed to favor the random search of final stable topologies. We do not expect to find a quantitative correspondence between the frequency of topologies in simulations and experiments. We regard only the final result of the model simulations; we have found a local equilibrium when the simulated shape no longer changes.

We compare this shape with the experimental results (topology, geometry). Distinguishing among topologies is trivial. However, because of the variability of membrane fluctuations, we find it difficult to describe the geometrical characteristics (e.g., contact angles for the mutant ommatidia, interface lengths, or elongation of cells) by quantitative measurements; one obtains more information by looking at the image ("eyeballing"). Quantitative measurements serve as a complement to eyeballing when enough data are available (cf. Fig. 1), not as a replacement. We determine for each model which parameters influence the shape of the C cells; for other parameters, we choose reasonable values (e.g., a compromise between simulation speed and precision; cf. ref. 25).

We assume that (*i*) adhesion strength is determined by the presence of these cadherins; when the two of them are present (i.e., at interfaces between C cells), adhesion is thus stronger. Mutants should be modeled by changing only existing parameters. We thus require that (*ii*) to model the *Roi*-mutants, we need only change the number of C cells; (*iii*) to model the cadherin mutant ommatidia, only the adhesion for the mutant cells should be changed (i.e., diminished for deletion, increased for overexpression); and (*iv*) all cells of a cell type that share the same mutation should be modeled by using the same parameter values.

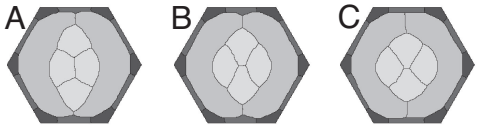

Fig. 2. Constant-tension model simulations. (*A*) $\gamma_{CC} = 4$, $\gamma_{CP} = \gamma_{PP} = 8$. (*B*) Same as *A* but with lower tension (stronger adhesion) between the polar and equatorial C cell, $\gamma_{\text{polar, equatorial}} = 2$. (*C*) Same as *A* but with lower tension (stronger adhesion) between the P cells: $\gamma_{PP} = 4$.

Constant Tension Model. A stronger adhesion between cells i and j is represented by a lower interfacial tension (13, 15–17), $\gamma_{ij} \geq 0$, which is a constant depending only on the cell types of i and j. We minimize the energy:

$$\varepsilon = \sum_{\text{interfaces}} \gamma_{ij} P_{ij} + \lambda_A \sum_{\text{cells}} (A_i - A_{0i})^2. \qquad [1]$$

P_{ij} is the length of the interface between cells i and j, A_i is the cell's area (the 2D equivalent of volume), A_{0i} is the cell's preferred area (target area), and λ_A is the area modulus (a lower value allows more deviations from A_0). The values of A_{0i} are inferred from the experimental pictures, with C cells being smaller than P cells. We assume C–C tension γ_{CC}, mediated by both E- and N-cadherin, to be weaker than C–P and P–P tension, γ_{CP} and γ_{PP}, which are mediated by E-cadherin alone. We assume the latter two to be equal: $\gamma_{CC} < \gamma_{CP} = \gamma_{PP}$. Only three parameters need be explored extensively: γ_{CC}, γ_{CP} ($= \gamma_{PP}$), and λ_A. The tensions γ influence the cell shapes directly, whereas λ_A determines a cell's deviations from the target area.

Starting the simulations with a four-cell vertex (SI Fig. 8*A*), we systematically find an incorrect topology (Fig. 2*A*): the anterior and posterior C cell touch. Even if we force the correct one, where the polar and equatorial C cells touch, it is unstable and decays into the incorrect one; the interfaces between the P cells are under tension and pull the polar and equatorial C cells apart.

To obtain the correct topology, we need another assumption: either that the adhesion between polar and equatorial C cells is stronger (Fig. 2*B*), or that the P cells pull less on them (by having a stronger adhesion; Fig. 2*C*). Still, the geometry is quite different from the experiments; notably, the interface between the polar and equatorial C cell is too short in simulations. Besides, there is no experimental evidence to support these assumptions.

Another optimization strategy is to determine (up to a prefactor) the tensions of three interfaces A, B, and D that meet in a vertex from the experimentally observed contact angles α, β, and δ ($\alpha + \beta + \delta = 360°$) by using $\gamma_A/\sin\alpha = \gamma_B/\sin\beta = \gamma_D/\sin\delta$ (12, 26). We inject those tensions in the model. By construction, we obtain the correct contact angles and thus topology, but the overall geometry (especially the interface lengths) differs considerably from observations (results not shown).

For the mutant ommatidia, requirements *ii*–*iv* mentioned above could not be satisfied with this model; there are too many cases where other parameters need to be changed as well. It would certainly be possible to choose a tension for each individual interface. However, if the tension was just an input parameter without biological basis, then the model would neither be predictive nor help us to understand the differences among the cells. We conclude that this model is insufficient to coherently describe the experiments.

Variable Tension Model. Adhesion between two cells tends to extend their contact length; it thus contributes negatively to the energy, $-J_{ij}P_{ij}$, where $J>0$; in agreement with intuition, a higher J describes a stronger adhesion, whereas $J = 0$ in the absence of adhesion (23, 24).

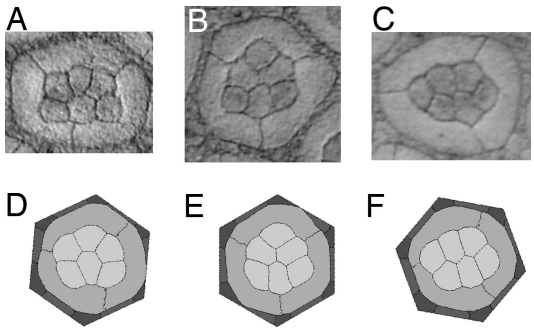

Fig. 3. *Roi*-mutants with six C cells. (*A–C*) Experimental pictures [*A* and *B* are reproduced with permission from ref. 9 (Copyright 2004, Nature Publishing Group).] (*D–F*) Corresponding simulations.

This extension is compensated by an elastic cell cortex term, $\lambda_P(P_i-P_{0i})^2$, where λ_P is the perimeter modulus, and P_{0i} is the target perimeter of cell i. The cell perimeter is the sum of its interfaces, $P_i = \Sigma_j P_{ij}$. We thus minimize the energy:

$$\varepsilon = -\sum_{\text{interfaces}} J_{ij}P_{ij} + \sum_{\text{cells}} [\lambda_P(P_i - P_{0i})^2 + \lambda_A(A_i - A_{0i})^2]. \quad [2]$$

The interfacial tension $\gamma_{ij} = \partial\, \varepsilon_{ij}/\partial P_{ij}$ between cells i and j is the energy change associated with a change in membrane length (cf. ref. 14); Eq. **2** yields:

$$\gamma_{ij} = -J_{ij} + 2\lambda_P(P_i - P_{0i}) + 2\lambda_P(P_j - P_{0j}). \quad [3]$$

As in the previous model, γ_{ij} is positive; otherwise, the cell would be unstable. However, it is no longer an input parameter. A stronger adhesion (high J) decreases the tension; this will usually cause an extension of the perimeter, which increases this tension again.

We represent all adhesion terms as combinations of E- and N-cadherin-mediated adhesion (J_E and J_N, respectively). In the wild type, the adhesion between C cells is mediated by both cadherins, so $J_{CC} = J_E + J_N$, whereas all other interfaces have only E-cadherin, so $J_{PP} = J_{CP} = J_E$. Values of A_0 are estimated from pictures. The target perimeter P_0 (expressed in units of $2\sqrt{\pi A_0}$) should be larger for cells that deviate more from a circular shape, i.e., for P cells. We thus adjust six main parameters: J_E, J_N, P_{0C}, P_{0P}, λ_P, and λ_A, which is too much to explore systematically. We adjust the parameters by hand for wild-type and mutant configurations simultaneously, because the wild type alone does not sufficiently constrain the number of optimal parameter combinations.

Unless indicated, throughout this paper and for all figures except Fig. 2, we use Eq. **2**, with the same set of parameters (SI Table 1) for wild type and mutants.

Wild Type. Starting the simulations with a four-cell vertex (SI Fig. 8*A*), the cells relax either into the correct topology where the polar and equatorial cells touch (Fig. 1) or into the incorrect one where anterior and posterior cells touch (analogous to Fig. 2*A*). Both topologies are stable, i.e., they are local energy minima.

In the correct topology, the geometry of the simulated ommatidium resembles well the experimental pictures. More quantitatively, the contact angles measured in simulations and experiments agree as well (Fig. 1). In contrast to the constant tension model, we do not need additional assumptions.

We found that the adhesion of secondary and tertiary pigment cells should be much stronger than can be expected from E-cadherin alone ($J_{23} > J_E$; SI Table 1), otherwise they lose contact. Experimentally, deleting the E-cadherin of these cells does not induce any geometrical or topological change (9). Both experiments and simulations thus suggest that secondary and tertiary pigment cells might have adhesion molecules other than E- and N-cadherin.

***Roi* Mutants.** With no additional parameter, we can simulate different numbers of C cells (*Roi*-mutants); the total size of the simulation lattice is adjusted accordingly. For one, two, three, and five C cells, only one topology is observed in experiments, and the same one is observed in simulations (SI Fig. 9).

For six C cells, three topologies are observed experimentally (Fig. 3 *A–C*). Theoretically, there are two more possible equilibrium topologies for six-cell aggregates, which are never observed, although one of them has a smaller total interface length (simulations using Surface Evolver; S. Cox, personal communication). We here performed a total of 42 Cellular Potts model simulations with different random seeds (see *Methods*) and found only three topologies (Fig. 3 *D–F*), which correspond to the observed ones.

We observe in Fig. 3 *A* and *C* that the entire ommatidium is elongated. Besides, ommatidia of *Roi*-mutants do not all have six sides and are assembled into a disordered pattern (see ref. 9). Thus, in *Roi*-mutants, ommatidia have variable shapes, the origin of which is not easily understood (especially for mutants with more pigment cells). Because in turn the shape of the ommatidium influences the geometry of its C cells (results not shown), studying the geometry of the C cells in more detail would by possible only by adding more free parameters.

N-Cadherin Mutants. Again without any additional parameter, simply by suppressing J_N, we could predict the pattern of ommatidia with N-cadherin-deficient C cells. Because N-cadherin is present only on interfaces between C cells, deletion

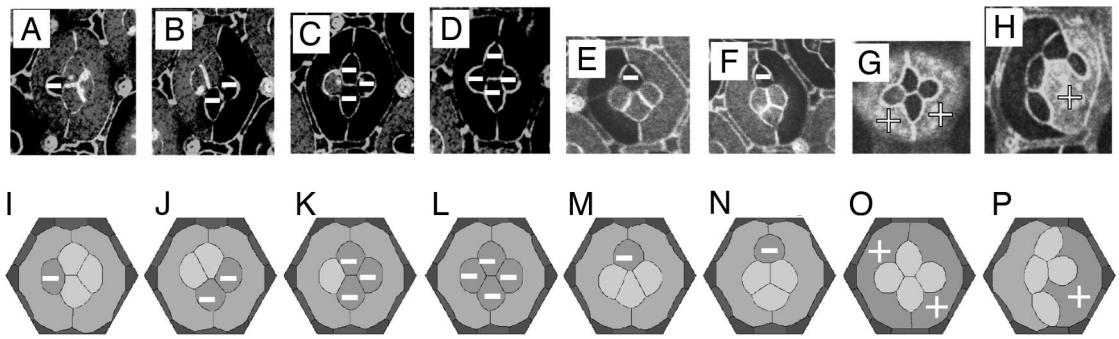

Fig. 4. N-cadherin mutants. Mutant cells are indicated with "+" for overexpression and "−" for deletion. (*A–H*) Experimental pictures. [*A–D* are reproduced with permission from ref. 9 (Copyright 2004, Nature Publishing Group).] (*I–P*) Corresponding simulations.

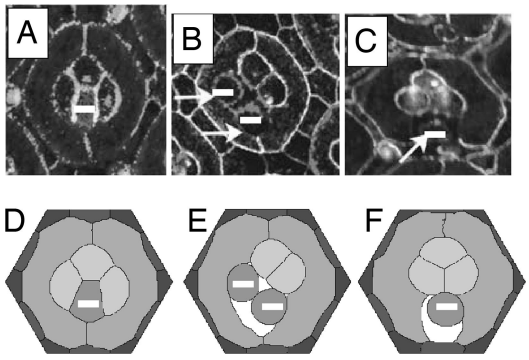

Fig. 5. Loss of adhesion. Mutant cells are indicated with ''−''. (*A*) A mutant C cell lacking E-cadherin. (*B* and *C*) Double-mutant C cells for E- and N-cadherin. (*D–F*) Corresponding simulations. [*A–C* are reproduced with permission from ref. 9 (Copyright 2004, Nature Publishing Group).]

means we set the adhesion between mutant and wild-type C cells as $J_{cC} = J_{cc} = J_E$ (mutant cells are denoted by lower-case letters).

We predict the correct topologies (Fig. 4 *A–F* and *I–N*), most of which are the same as in wild type. We predict qualitatively the main geometrical differences between mutants and wild type: (*i*) the length of the interfaces between mutant and wild-type C cells decreases; (*ii*) the contact angles change; (*iii*) the interface length between the remaining wild-type C cells increases (Fig. 4 *A* and *B* and *I–J*); and (*iv*) the length of the central interface increases (Fig. 4 *D* and *L*).

When the polar or equatorial cell is the only C cell without N-cadherin, we simulate (Fig. 4 *M* and *N*) both topologies that coexist in experiments (Fig. 4 *E* and *F*).

To simulate one mutant P cell that misexpresses N-cadherin, we optimize J_{Cp}. Ectopic expression of N-cadherin results induces a high-level expression of N-cadherin. Therefore, whereas for wild-type $J_{CP} = J_E = 150$, we find an increase for the mutant, $J_{Cp} = 150 + 600$. The high adhesion of this P cell with the C cells severely disrupts the normal configuration. Many topologies that differ considerably from the wild type are observed in experiments and simulations (e.g., Fig. 4 *H* and *P*). When both P cells misexpress N-cadherin, they balance each other, and the topology is back to normal (Fig. 4*G*). Optimization yields $J_{pp} = 150 + 700$ (Fig. 4*O* and SI Fig. 10). Both J_{Cp} and J_{pp} are higher than the wild-type value of *C–C* adhesion ($J_{CC} = J_E + J_N = 150 + 450$).

E-Cadherin Mutants. The mutant C cell in Fig. 5*A* does not express E-cadherin, and it lacks adherens junctions at the interfaces with the P cells (9). To simulate it, it would seem natural to suppress J_E at all interfaces; that is, $J_{cP} = 0$ and $J_{cC} = J_N$. With this assumption, we obtain the correct topology, which is the same as in the wild type; however, the simulated geometry (not shown) is also the same as the wild type, whereas the experiment is significantly different (Fig. 5*A*). If we rather assume that *C–C* adhesion is unchanged by this mutation ($J_{cC} = J_{CC}$), we obtain a good agreement (Fig. 5*D*).

E-cadherin overexpression in C cells (but not in P cells) significantly affects the pattern, yielding a coexistence of different topologies: in Fig. 6 *A* and *B*, the same cells are mutants, but the topologies differ; the same holds for Fig. 6 *D* and *E*. We predict the observed topologies (all stable) and, qualitatively, the geometries (Fig. 6 *F–J*) when we increase the C–P cell adhesion from $J_{CP} = J_E = 150$ to $J_{cP} = 300$; although we find that the adhesion between wild-type and mutant C cells should not change, $J_{cC} = J_{CC} = J_E + J_N$, we should change it if both are mutants, $J_{cc} = 350 + J_N$. Because E-cadherin overexpression in P cells rarely induces geometrical or topological changes (9), we do not change their adhesion values.

E- and N-Cadherin Mutants. We predict the effect of both E- and N-cadherin missing in C cells by setting $J_{cC} = J_{cP} = J_{cc} = 0$. Mutant C cells do not adhere to any of their neighbors (Fig. 5 *E* and *F*); intercellular space becomes visible between the cells, and the cells have shrunk. This agrees well with experiments, where mutant C cells lose the apical contacts with their neighbors (Fig. 5 *B* and *C*).

Discussion

Constant and Variable Tension Models. When surface tension is a constant model parameter, modified only by adhesion, the surface mechanics are soap-bubble-like: minimization of the interfaces with cell-type-dependent weights (13, 15–17, 27). This model proves to be insufficient here. However, in studies focusing on larger aggregates (10^2 to 10^4 cells) (17, 27, 28), constant surface tension was sufficient to explain tissue rounding and cell sorting and even *Dictyostelium* morphogenesis (29). This constant-tension model catches two important features of tissues of adherent cells: first, cells tile the space without gaps or overlap; second, the interface between cells is under (positive) tension, which implies, for instance, that three-cell vertices are stable unlike four-cell ones (10, 11), thus severely constraining the possible topologies (11).

In the present example of retina development, we show that interfacial tension should be variable, as described in a second model (23, 24). Tension results from an adhesion-driven extension of cell–cell interfaces, balanced by an larger cortical tension (Eq. **3**). It explains correctly the topologies of many observations and correctly simulates the geometries. It requires more free parameters, but they are tested against many more experimental data; and their origins, signs, and variations are biologically relevant (14).

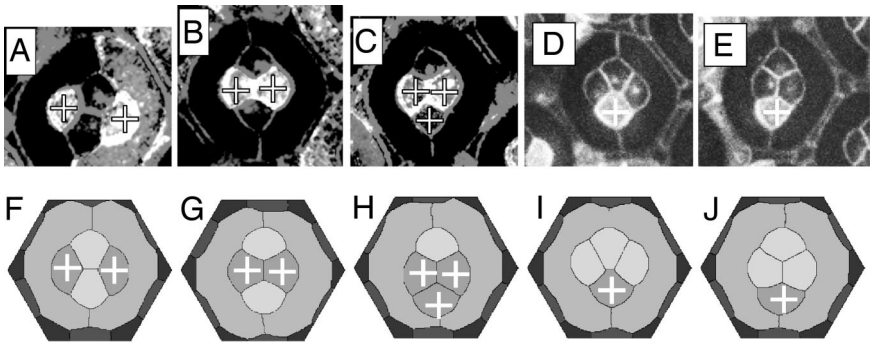

Fig. 6. E-cadherin overexpression. Mutant cells are indicated with ''+''. (*A–E*) Experimental pictures [*A–C* are reproduced with permission from ref. 9 (Copyright 2004, Nature Publishing Group).] (*F–J*) Corresponding simulations.

Adding more refinements (and thus more free parameters) is possible but does not seem necessary to describe the equilibrium shape of ommatidial C cells. The parameters should not be taken as quantitative predictions, because *in vivo* biophysical measurements for calibration are lacking.

Adhesion. By adjusting a set of six independent free parameters in this variable tension model, we obtain topological and geometrical agreement between the simulations and the pictures of 16 different situations: the wild type (Fig. 1) and the six topologies observed in the *Roi*-mutants (Fig. 3 and SI Fig. 9), as well as the nine cadherin deletion mutants (Figs. 4 *A–F* and 5) by setting the corresponding parameter to zero.

We also simulate seven cadherin overexpression mutants by readjusting the corresponding parameter (Figs. 4 *G* and *H* and 6): adhesion is increased. The strongest increases are found when two overexpressing cells touch; this corresponds to the idea that the adhesion strength depends on the availability of cadherin molecules in both adhering cells.

We found two cases where a mutation does not seem to change adhesion strength: first, when deleting E-cadherin from one C cell, its adhesion with a normal C cell is unchanged (Fig. 5*D*); second, we rarely observed shape changes in E-cadherin-overexpressing P cells in experiments (cf. ref. 9).

Indeed, whereas a linear relation between cadherin expression and adhesion strength has been found *in vitro* (30), this need not be true *in vivo*, because cells have many more ways to regulate protein levels. These exceptions thus do not contradict the conclusion that the shapes observed in mutants are the effect of altered adhesion: an increase in the case of overexpression, a decrease in the case of deletion.

Cortical Tension. In the variable tension model, the perimeter modulus λ_P and the target perimeter P_0 reflect the role of the cortical cytoskeleton. The target perimeter is always smaller than the perimeter; therefore, the interfacial tension γ_{ij} (Eq. **3**) is always positive; otherwise, the cell would be unstable and fall apart. The cortex of the simulated cells is contractile and generates tension. This tension depends on the perimeter P of the cell, the length of which depends on the cell's shape, which in turn depends on the tension; there is feedback between tension and shape and thus between each cell and its neighbors.

To understand the effect of this feedback, let us consider the wild-type ommatidium. We assume that the four C cells have equal adhesion properties. The tension at the interfaces between the two P cells pulls at the polar and equatorial C cell. When the tension is constant, these cells will therefore be pulled apart (Fig. 2*A*): the cells do not react on their deformation. However, when the tension depends on the cell's perimeter, pulling at those cells deforms them and increases their tension: energy minimization thus requires they stay in contact.

The prediction that cytoskeletal contractility is essential for the establishment of cell shape should be tested, e.g., by treating the cells with cytoskeletal inhibitors (19, 31) or by genetically modifying the cytoskeleton. Because the cytoskeleton has multiple functions that could interfere with adhesion (cf. refs. 6 and 32), the results will be difficult to interpret. Preliminary experimental results (not shown) indicate that genetically disturbing Rho-family GTPases influences the cell shape. The role of the cytoskeleton has been confirmed in various tissues and organisms (see refs. 14 and 33 for reviews). We here present a computational framework able to test this hypothesis, which can be extended to other tissues, ranging from the patterns of a few cells to large-scale aggregates.

Methods

Experiments. Retinas were stained and analyzed as described in refs. 9 and 34. In short, cells were stained with cobalt sulfide (Fig. 3 and SI Fig. 9) to visualize the cell membrane, or stained with fluorescently labeled antibodies against DE-cadherin, DN-cadherin (referred to as E- and N-cadherin, respectively, in the rest of the text), β-catenin, or β-spectrin for confocal microscopy. Rough-eye (*Roi*) flies were used to examine the topology and geometry of variable number of C cells. The effect of eliminating or overexpressing cadherin molecules was studied in mosaic retinas composed of wild-type and mutant cells generated by the FLP-out method (see ref. 9). We examined more than five retinas in each experiment. Thus, at least several hundred ommatidia (>500) were examined for the wild type and each mutation, except E- and N-cadherin overexpression, in which case ≈100 ommatidia were examined. Some pictures used for the analysis were published previously (9, 34).

Model Simulations. The cellular Potts model (15, 16) is a standard algorithm to simulate variable cell shape, size, and packing (25). Its use in biology is motivated by the capability to handle irregular fluctuating interfaces (cf. ref. 35); the pixelization induced by the calculation lattice can be chosen to correspond to the pixelization in the experimental images.

Each cell is defined as a certain set of pixels, here on a 2D square lattice; their number defines cell area A. The cell shapes change when one pixel is attributed to one cell instead of another. Our field of simulation for one ommatidium is a hexagon with sides of ≈100 pixels (its surface is $A_{\mathrm{hex}} = 25{,}160$ pixels, about the same as in experimental pictures). We use periodic boundary conditions, as if we were simulating an infinite retina with identical ommatidia. Initially, the whole hexagon is filled with cells, approximately at the right positions (SI Fig. 8). We treat bristle cells as tertiary pigment cells; both are situated at the edge of three ommatidia. These initial conditions, with an unstable n-cell vertex in the middle, do not fix the final configuration in advance. Simulations can be started with different seeds of the random number generator to explore whether multiple solutions are possible.

Shape is relaxed to decrease the energy ε, Eqs. **1** (15) or **2** (24). The algorithm to minimize ε uses Monte Carlo sampling and the Metropolis algorithm, as follows. We randomly draw (without replacement) a lattice pixel and one of its eight neighboring pixels. If both pixels belong to different cells, we try to copy the state of the neighboring pixel to the first one. If the copying diminishes ε, we accept it, and if it increases ε, we accept it with probability $P = \exp(-\Delta\varepsilon/T)$. Here $\Delta\varepsilon$ is the difference in ε before and after the considered copying. The prefactor T is a fluctuation (random copying) allowance; it determines the extent of energy-increasing copy events, leading to membrane fluctuations (35). Because all energy parameters are scalable with the fluctuation allowance T, we can fix it without loss of generality; for numerical convenience, we choose numbers on the order of 100.

We define one Monte Carlo time step (MCS) as the number of random drawings equal to the number of lattice pixels. It takes ≈600–4,000 MCS to attain a shape that no longer evolves, that is, in mechanical equilibrium where stresses are balanced. We run the simulation much longer (up to 10^6 MCS) to test whether topological changes occur.

To avoid possible effects of lattice anisotropy on cell shapes, we compute P and ε by including interactions up to the 20 next-nearest neighbors (36). All perimeters indicated here are corrected by a suitable prefactor 10.6 to ensure that a circle with an area of A pixels has a perimeter $2\sqrt{\pi A}$ (37).

In experiments, interstitial fluid is present in small amounts, and cells can lose contact (Fig. 5 *B* and *C*). To simulate it in our 2D model, at each MCS, we randomly choose one pixel at a cell interface and change its state into "intercellular space" (a state without adhesion or area and perimeter constraints). In addition, we choose the sum of all cells target areas to be less than the total

size of the hexagonal simulation field ($\Sigma_{\text{cells}} A_{0i} = 0.95\, A_{\text{hex}}$; SI Table 1). Only when cells lose adhesion ($J = 0$) do we actually observe intercellular space in simulations (Fig. 5 *E* and *F*).

We try different parameters and adjust them to improve visual agreement (eyeballing) between simulated and experimental pictures. To estimate our uncertainty, we note that 5−10% changes in the values of the adhesion parameters do not yield visible changes in the geometry, whereas 10−30% changes do; see SI Fig. 10 for an example of the determination of J_{Cp}.

Images. Once we simulate the correct topology, we measure the contact angles of straight lines fitted through the interfaces that meet in the vertex. The line should be long enough to avoid grid effects; we fit a straight line using the first 15 first-order neighboring sites. Because the simulated cells show random fluctuations, statistics are obtained by measuring the contact angles several times during the simulation or in simulations with different random-number seeds. In experimental pictures (cover picture of ref. 34), we measure contact angles in 22 wild-type ommatidia by hand, aided by the program ImageJ (38). Ommatidia have two axes of symmetry, and we consider the ommatidia to consist of four equal quarters, which gives us 88 measurements for each angle (and 44 measurements of the angles intersected by the axes of symmetry). The variation between different wild-type ommatidia is larger than in simulations (Fig. 1). In mutant ommatidia, the error bar is even larger, so we did not attempt any quantitative comparison.

We thank Simon Cox for Surface Evolver calculations on soap-bubble clusters, Christophe Raufaste for discussions on computational methods, Sascha Hilgenfeldt for interesting discussions, and Yohanns Bellaïche for critical reading of the manuscript. We thank T. Uemura, H. Oda, U. Tepass, G. Thomas, B. Dickson, P. Garrity, the Bloomington *Drosophila* Stock Center, and the Developmental Studies Hybridoma Bank for fly strains and/or antibodies; and K. Saigo for use of facilities. T.H. was supported by a research fellowship from the Japan Society for the Promotion of Science for Young Scientists.

1. Steinberg MS (1963) *Science* 141:401–408.
2. Niewiadomska P, Godt D, Tepass U (1999) *J Cell Biol* 144:533–547.
3. Foty RA, Steinberg MS (2004) *Int J Dev Biol* 48:397–409.
4. Lecuit T (2005) *Trends Cell Biol* 15:34–42.
5. Classen AK, Anderson KI, Marois E, Eaton S (2005) *Dev Cell* 9:805–817.
6. Gumbiner BM (2005) *Nat Rev Mol Cell Biol* 6:622–634.
7. Carthew RW (2005) *Curr Opin Genet Dev* 15:358–363.
8. Wolff T, Ready D (1993) in *The Development of Drosophila melanogaster*, eds Bate M, Martinez Arias A (Cold Spring Harbor Laboratory Press, Cold Spring Harbor, NY), pp 1277–1325.
9. Hayashi T, Carthew RW (2004) *Nature* 431:647–652.
10. Plateau J (1873) *Statique Expérimentale et Théorique des Liquides Soumis aux Seules Forces Moléculaires* (Gauthier-Villars, Paris), Vol 1.
11. Weaire D, Hutzler S (1999) *The Physics of Foams* (Oxford Univ Press, Oxford, UK).
12. Thompson D (1942) *On Growth and Form: A New Edition* (Cambridge Univ Press, Cambridge, UK); reprinted (1992) (Dover, New York).
13. Chichilnisky EJ (1986) *J Theor Biol* 123:81–101.
14. Lecuit T, Lenne PF (2007) *Nat Rev Mol Cell Biol* 8:633–644.
15. Graner F, Glazier JA (1992) *Phys Rev Lett* 69:2013–2016.
16. Glazier JA, Graner F (1993) *Phys Rev E* 47:2128–2154.
17. Graner F (1993) *J Theor Biol* 164:455–476.
18. Sheetz MP, Dai J (1996) *Trends Cell Biol* 6:85–89.
19. Raucher D, Sheetz MP (1999) *Biophys J* 77:1992–2002.
20. Dai J, Sheetz MP (1999) *Biophys J* 77:3363–3370.
21. Morris CE, Homann U (2001) *J Membr Biol* 179:79–102.
22. Thoumine O, Cardoso O, Meister JJ (1999) *Eur Biophys J* 28:222–234.
23. Graner F, Sawada Y (1993) *J Theor Biol* 164:477–506.
24. Ouchi NB, Glazier JA, Rieu JP, Upadhyaya A, Sawada Y (2003) *Phys A* 329:451–458.
25. Marée AFM, Grieneisen VA, Hogeweg P (2007) in *Single Cell Based Models in Biology and Medicine*, eds Anderson ARA, Chaplain MAJ, Rejniak KA (Birkhäuser, Basel), pp 107–136.
26. Langmuir I (1933) *J Chem Phys* 1:756–776.
27. Brodland GW, Chen HH (2000) *J Biomech Eng* 122:402–407.
28. Käfer J, Hogeweg P, Marée AF (2006) *PLoS Comput Biol* 2, e56.
29. Marée AFM, Hogeweg P (2001) *Proc Natl Acad Sci USA* 98:3879–3883.
30. Foty RA, Steinberg MS (2005) *Dev Biol* 278:255–263.
31. Bar-Ziv R, Tlusty T, Moses E, Safran SA, Bershadsky A (1999) *Proc Natl Acad Sci USA* 96:10140–10145.
32. Geisbrecht ER, Montell DJ (2002) *Nat Cell Biol* 4:616–620.
33. Schock F, Perrimon N (2002) *Annu Rev Cell Dev Biol* 18:463–493.
34. Hayashi T, Kojima T, Saigo K (1998) *Dev Biol* 200:131–145.
35. Mombach JC, Glazier JA, Raphael RC, Zajac M (1995) *Phys Rev Lett* 75:2244–2247.
36. Holm EA, Glazier JA, Srolovitz DJ, Grest GS (1991) *Phys Rev A* 43:2662–2668.
37. Raufaste C (2007) PhD thesis (Université Joseph Fourier, Grenoble, France).
38. Rasband WS (2005) *ImageJ* (National Institutes of Health, Bethesda, MD), Ver 1.34s, http://rsb.info.nih.gov/ij.